

PACS №: 41.20Jb; 84.40Xb

Malek G. M. Hussain

Electrical Engineering Department, Kuwait University

P.O. Box 5969, Safat 13060, Kuwait

Telephone: (965) 481-6467, Fax: (965) 481-7451,

e-mail: malek@kuc01.kuniv.edu.kw

# Waveform Design and Generalized Ambiguity Function for Ultrawideband Nonsinusoidal Signals

## Contents

<b>1. Introduction</b>	<b>36</b>
<b>2. Nonsinusoidal Waveform Design</b>	<b>37</b>
2.1. Generalized Gaussian Pulse . . . . .	37
2.2. Sidelobe Canceller . . . . .	39
2.3. Ultrawideband Coded Signals . . . . .	39
2.4. Doppler-Effect of Carrier-Free Signals . . . . .	40
<b>3. Generalized Ambiguity Function</b>	<b>41</b>
<b>4. Characteristics of the Generalized Ambiguity Function</b>	<b>42</b>
<b>5. Conclusions</b>	<b>43</b>
<b>Appendix A.</b>	<b>43</b>
<b>Appendix B.</b>	<b>45</b>

## Abstract

The classical theory of radar resolution is based on narrowband sinusoidal waveforms and cannot directly be applied to ultrawideband (UWB) impulse radar. The concept of a generalized ambiguity function, which is a two-dimensional autocorrelation function in the range-Doppler domain, was first introduced by Harmuth in 1981 as a convenient design tool for the performance analysis of carrier-free radar. In 1989, we derived a generalized ambiguity function for coded waveforms represented by a sequence of (positive and negative) ideal Gaussian pulses. In this paper, the concepts of waveform design and ambiguity function are presented based on a physically realizable nonsinusoidal signal. The time variation of the nonsinusoidal signal is that of a generalized Gaussian pulse (GGP) having UWB frequency spectrum that is free from dc component. Therefore, the GGP signal can be radiated by a broadband antenna. For resolution enhancement, a sidelobe canceller is devised to eliminate the undesirable sidelobes of the autocorrelation function of the GGP signal without any significant reduction in signal energy. The generalized ambiguity function for UWB coded signals that are composed of a finite sequence of GGP signals is derived too. Computer plots of the generalized ambiguity function are generated for different design parameters. The plots demonstrate to what extent the generalized ambiguity function of the coded GGP signals can achieve the target resolution and clutter suppression capabilities of an ideal thumbtack ambiguity function.

## 1. Introduction

The rapid technological advances during the last two decades of the 20<sup>th</sup> century have made it possible for ultrawideband (UWB) radio-transmission

technology to emerge. UWB radar is classified into two categories: (1) radar system operating with a sinusoidal carrier and a large relative bandwidth, and (2) carrier-free radar system utilizing ultrashort (baseband) pulses referred to as nonsinusoidal waves

or impulses [1]–[3]. The concept of relative bandwidth was introduced by Harmuth [1] to distinguish between narrowband and ultrawideband radio technology. The relative bandwidth is defined as follows:

$$\begin{aligned} \eta &= \frac{\Delta f}{f_c} && \text{for sinusoidal signals,} \\ \eta &= \frac{f_H - f_L}{f_H + f_L} && \text{for nonsinusoidal signals} \end{aligned} \quad (1)$$

where  $\Delta f$  is absolute bandwidth,  $f_c$  carrier frequency, and  $f_H$  and  $f_L$  are the highest and the lowest frequency of interest. The terms relative bandwidth and *fractional bandwidth* that is more commonly used in the UWB radar literature are synonymous; for carrier-free nonsinusoidal signals fractional bandwidth equals  $2\eta$ . UWB radar has been defined so far as a radar system having a fractional bandwidth larger than 0.25 [2].

The applications of UWB radar are numerous [1], [2]. Achieving high-resolution capabilities is one of the most important advantages of UWB radar. The ambiguity function is an essential design tool for the performance evaluation of radar signals and systems in terms of target resolution, target detection in the presence of additive white Gaussian noise, and clutter and interference rejection. The mathematical formulation of the classical ambiguity function, based on the complex representation of narrow-band signals, was first introduced by Ville in 1948 [4]. In 1953, Woodward applied the concept of the ambiguity function to the field of radar resolution [5]. The classical ambiguity function for a narrow-band complex signal

$$s(t) = u(t)e^{j2\pi f_0 t}, \quad u(t) = |u(t)|e^{j\phi(t)}, \quad (2)$$

where  $u(t)$  is the complex envelope, and  $f_0$  is the carrier frequency, is given by the integral relationship

$$\chi(\tau, \nu) = \int_{-\infty}^{+\infty} u(t)u^*(t - \tau)e^{j2\pi\nu t} dt \quad (3)$$

In (3), the asterisk (\*) denotes complex conjugate, and the variables  $\tau$  and  $\nu$  denote the *delay* and *Doppler* coefficients, respectively.

An ideal ambiguity function is a single spike, with no sidelobes, centered in the range-Doppler domain. It is referred to in the radar literature as “thumbtack ambiguity function”. Its physical realization would yield superior target-resolution and clutter-rejection capabilities for radar. Extensive research efforts have gone into finding radar signals, with the structure given in (2), that can produce ambiguity functions having characteristics close to that of the ideal thumbtack ambiguity function [6–10]. Harmuth [1, 11] and Hussain [12] have demonstrated that the desired thumbtack ambiguity function can be achieved by UWB nonsinusoidal coded waveforms.

The ambiguity functions presented in [1] and [11] are for nonsinusoidal coded waveforms that are composed of a sequence of ideal *rectangular* pulses, and the ones presented in [12] are for Barker codes, complementary codes, and pseudo-random (PN) codes that are composed of a sequence of ideal *Gaussian* pulses. The ideal rectangular and Gaussian pulses are not physically realizable, and their frequency spectrum includes a dc component which prevents their emission (in the form of electromagnetic signals) by an antenna.

In this paper, the radar-resolution theory introduced in [12] is revised for a physically realizable signal model, referred to as the *generalized Gaussian pulse* (GGP) [13]. The GGP is an UWB signal having an attractive autocorrelation function and an energy spectrum that is free from a dc component. A generalized ambiguity function will be derived for nonsinusoidal coded waveforms that are represented by a sequence of GGP signals with the combined *amplitude-shift coding* and *pulse-position coding*. The resolution and the clutter-suppression capabilities of the coded signals will be investigated by generating computer plots of the generalized ambiguity function for different coding structures and signal parameters.

The concepts of carrier-free signal design, Doppler effect, and sidelobe cancellation are described in Section 2. In Section 3, the classical matched-filter theory is used to derive generalized ambiguity function for nonsinusoidal coded signals having a hyperfine structure of GGP. In Section 4, computer plots of generalized ambiguity functions are presented for different signal parameters. Conclusions are given in Section V. In Appendix A and Appendix B, detailed derivation of the Doppler effect associated with UWB Gaussian pulses reflected from a moving target is presented.

## 2. Nonsinusoidal Waveform Design

One of the intricate and challenging tasks in the design of UWB impulse radar is the generation and transmission of energy-efficient electromagnetic signals that can yield reliable target detection and resolution, in the presence of clutter and interference. In analogy to the narrowband complex-signal representation used in the classical theory of radar and radio communications, we shall present a realistic and (mathematically) convenient signal model for the theory and analysis of UWB impulse radar.

### 2.1. Generalized Gaussian Pulse

A signal model that is well suited for the representation of carrier-free electromagnetic signals

used in practice for impulse radar and radio communications is the GGP signal model defined analytically by the time function,

$$\Omega(t) = \frac{E_o}{1-\alpha} \left( \exp\{-4\pi[(t-t_o)/\Delta T]^2\} - \alpha \exp\{-4\pi[\alpha(t-t_o)/\Delta T]^2\} \right), \quad \alpha \neq 1. \quad (4)$$

In (4),  $E_o$  is the peak amplitude at the time  $t = t_o$ ,  $\Delta T$  is nominal duration, and  $\alpha$  is a scaling parameter that shapes the frequency density spectrum of the GGP signal. The function  $\Omega(t)$  is referred to as the *generalized Gaussian pulse* (GGP).

The autocorrelation function  $\Upsilon(t)$  of the GGP signal is expressed as follows,

$$\Upsilon(t) = \int_{-\infty}^{+\infty} \Omega(\lambda)\Omega(\lambda+t) d\lambda = E_o^2 \Delta T \sum_{k=0}^2 I_k \exp\{-a_k[(t-t_o)/\Delta T]^2\}, \quad (5)$$

where

$$\begin{aligned} I_0 &= \frac{1}{\sqrt{8}(1-\alpha)^2}, \\ I_1 &= \frac{\alpha}{\sqrt{8}(1-\alpha)^2}, \\ I_2 &= -\frac{\alpha}{(1-\alpha)^2(1+\alpha^2)^{1/2}}, \\ a_0 &= 2\pi, \quad a_1 = 2\pi\alpha^2, \quad a_2 = \frac{4\pi\alpha^2}{(1+\alpha^2)}. \end{aligned} \quad (6)$$

The energy spectral density  $\Psi(f)$  of the GGP signal  $\Omega(t)$  is defined as the Fourier transform of the autocorrelation function  $\Upsilon(t)$ ,

$$\begin{aligned} \Psi(f) &= \int_{-\infty}^{+\infty} \Upsilon(t) \exp\{-j2\pi ft\} dt \\ &= \left( \frac{E_o}{\Delta f} \right)^2 \exp\{-j2\pi t_o(f/\Delta f)\} \\ &\quad \times \sum_{k=0}^2 \sqrt{\frac{\pi}{a_k}} I_k \exp\left\{-\frac{\pi^2}{a_k}(f/\Delta f)^2\right\}, \end{aligned} \quad (8)$$

where  $\Delta f = 1/\Delta T$  is the effective frequency bandwidth of the GGP. The energy  $\mathcal{E}$  of the GGP signal  $\Omega(t)$  can be determined from the peak value of its autocorrelation function at  $t = t_o$ ,

$$\begin{aligned} \mathcal{E} = \Upsilon(t_o) &= \frac{E_o^2 \Delta T}{\sqrt{8}(1-\alpha^2)} \\ &\quad \times \left[ 1 + \alpha - \left( \frac{8\alpha^2}{1+\alpha^2} \right)^{1/2} \right], \quad \alpha \neq 1. \end{aligned} \quad (9)$$

Plots of the normalized GGP signal  $\Omega(t)/E_o$ , autocorrelation function  $\Upsilon(t)/\Upsilon(0)$ , and energy

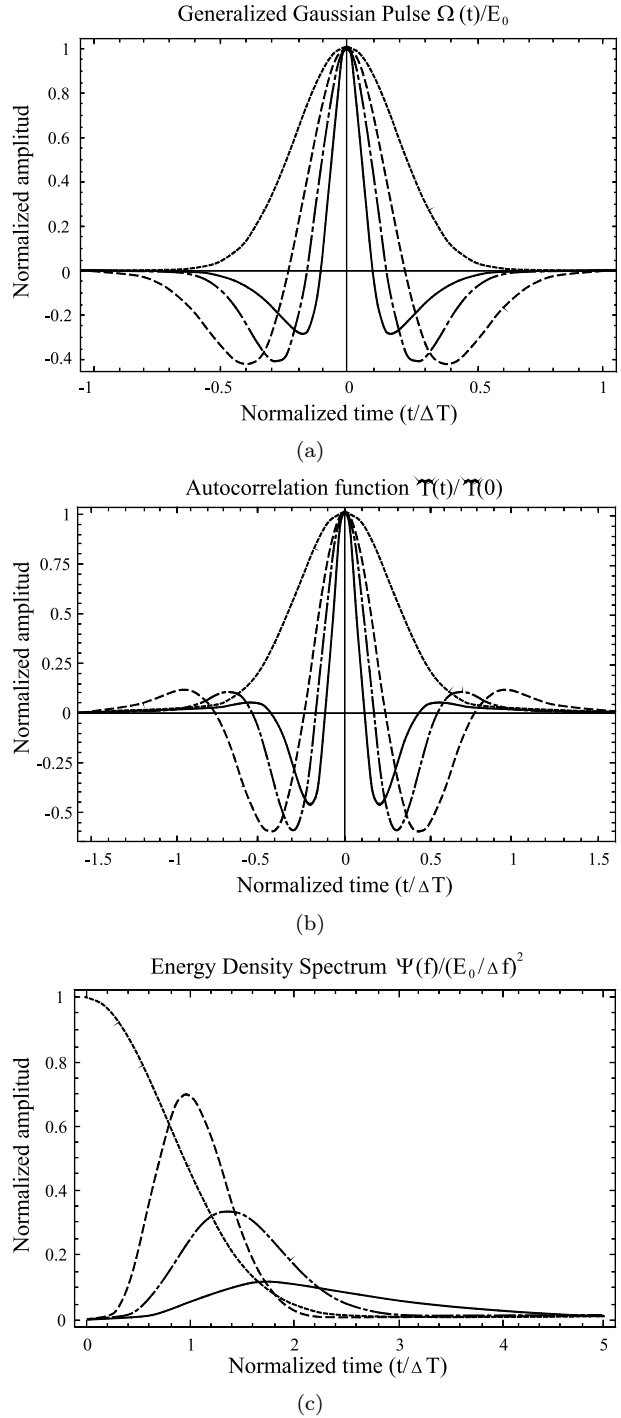


Fig. 1. Normalized time variation of the generalized Gaussian pulse  $\Omega(t)/E_o$  (a), autocorrelation function  $\Upsilon(t)/\Upsilon(0)$  (b), and energy density spectrum  $\Psi(f)/(E_o/\Delta f)^2$  (c), for values of the scaling parameter  $\alpha = 0$  (dotted line),  $\alpha = 0.75$  (dashed line),  $\alpha = 1.5$  (dashed-dotted line), and  $\alpha = 3$  (solid line).

density spectrum  $\Psi(f)/(E_o/\Delta f)^2$  are shown in Fig. 1(a), (b), and (c), respectively. The plots are computed for the value of the time constant  $t_o = 0$ , and the values of the scaling factor  $\alpha = 0$

(dotted line), 0.75 (dashed line), 1.5 (dashed-dotted line), and 3 (solid line). According to Fig. 1(a), the GGP is characterized by a mainlobe and two distinguishable sidelobes of negative amplitudes. For  $\alpha = 0$ , the sidelobes disappear and the GGP reduces to an ideal Gaussian pulse, with a Gaussian-shape autocorrelation function too, and an energy density spectrum that includes dc component as shown by the dotted lines in Fig. 1.

For the increasing values of  $\alpha$  in the range  $0 < \alpha < 1$ , the duration of the GGP and that of its autocorrelation function decreases while the magnitudes of their time-sidelobes increase. Time-sidelobes of large magnitudes are not desirable for target resolution. For  $\alpha > 1$ , the duration as well as sidelobe levels become decreasing functions of  $\alpha$ . The effective bandwidth of the energy density spectrum in Fig. 1(c) is an increasing function of  $\alpha$  too. Hence, larger values of the scaling factor  $\alpha > 1$  are more attractive for improved resolution capabilities.

One of the most important features of the GGP signal that must be highlighted is the fact that its energy spectrum  $\Psi(f)$  is free from dc component for  $\alpha \neq 0$ ;  $\Psi(0) = 0$ . According to antenna theory and practice, only charge acceleration through a radiating surface results in the radiation of an electromagnetic field. Thus, a dc component would not generate an electromagnetic field. This principle puts no restrictions on the radiation of electromagnetic signals having the time variation of the GGP signal given in (4). In fact, the radiation of electromagnetic signals having the time variation of a GGP has been achieved in practice [14, 15].

## 2.2. Sidelobe Canceller

The performance of radar target detection is determined in terms of the available signal energy at the output of the matched-filter receiver, or correlator receiver, while the characteristics of the signal autocorrelation function, e.g., effective width of mainlobe and amplitude of sidelobes, affect the resolution capability of the radar. The negative time sidelobes of the autocorrelation function  $\Upsilon(t)$  in Fig. 1(b) can be eliminated, without loss of signal energy, by employing at the output of the correlator receiver a “sidelobe canceller” that is composed of a full-wave rectifier and an adder (or summer) as shown in Fig. 2. According to Fig. 2, for an input GGP signal,  $\Omega(t)$ , the output of the correlator is the autocorrelation signal  $\Upsilon(t)$ , the output of the full-wave rectifier is the absolute value of the signal  $\Upsilon(t)$ , which is denoted by  $|\Upsilon(t)|$ , and the output of the summer circuit is the improved autocorrelation signal

$$\Theta(t) = \Upsilon(t) + |\Upsilon(t)| \quad (10)$$

shown in Fig. 3 for the value  $\alpha = 3$ . According to Fig. 3, the peak amplitude of the signal  $\Theta(t)$  is

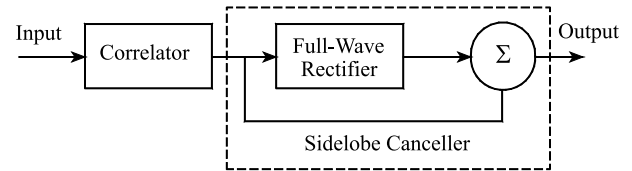


Fig. 2. Correlator and sidelobe canceller that is composed of a full-wave rectifier and an adder, for improving the characteristics of the autocorrelation function of the generalized Gaussian pulse shown in Fig. 1.

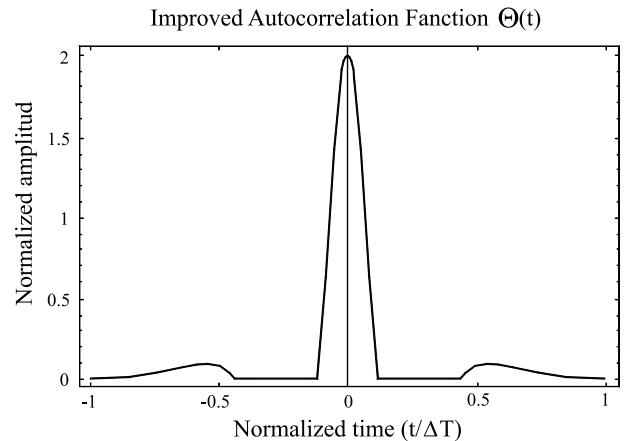


Fig. 3. Improved autocorrelation function  $\Theta(t) = (|\Upsilon(t)| + \Upsilon(t))/\Upsilon(0)$  at the output of the sidelobe canceller in Fig. 2. The input signal is the GGP  $\Omega(t)$  with the scaling factor  $\alpha = 3$ .

twice that of  $\Upsilon(t)$  shown in Fig. 1(b), and its time variation is free from the large negative sidelobes. Note that the energy content in the mainlobe of the signal  $\Theta(t)$  accounts for the loss of energy from the original signal  $\Upsilon(t)$  due to sidelobe cancellation. Hence, the performance of target detection is not affected by the sidelobe canceller.

A bank of correlator receivers and sidelobe cancellers configured as shown in Fig. 2 is suitable for generating the generalized ambiguity function for nonsinusoidal coded signals [12]. The generalized ambiguity function for UWB coded waveforms that are composed of a sequence of GGP signals will be derived in Section 3. In Section 4, we shall demonstrate how the characteristics of the generalized ambiguity function can significantly be enhanced to match that of the so called thumbtack ambiguity function by employing the receiver system in Fig. 2.

## 2.3. Ultrawideband Coded Signals

The inherent low-energy content of an electromagnetic impulse limits the maximum detection range of ultrawideband impulse radar. The use of a (coded) sequence of  $N$  electromagnetic impulses, each having the energy content  $\mathcal{E}$ , can

enhance the energy level required for a reliable target detection by a factor  $N$ . Furthermore, by properly amplitude-shift coding and/or staggering the pulse-repetition interval (PRI) of the sequence of impulses, one can achieve a spread-spectrum radar signal with *low probability of intercept*, and protection against jamming and interference. A convenient spread-spectrum signal model for the applications of carrier-free radar and radio communications is structured as follows [16]- [18]:

$$s(t) = \sum_{n=0}^{N-1} q_n \Omega_n(t - nT_r - \varepsilon_n T_c). \quad (11)$$

In (11), the component pulse  $\Omega_n(t)$  is a GGP with scaling factor  $\alpha_n \neq 1$ ,  $\{q_n\}$  is a sequence of +1's and -1's corresponding to a binary code of length  $N$ ,  $T_r$  is PRI,  $\{\varepsilon_n\}, 0 \leq |\varepsilon_n| \leq Q$  (an integer), is a *pseudo-random* (PN) *time-hopping* sequence for staggering the PRI by shifting the component pulse at the  $n^{th}$  position by an additional period  $\varepsilon_n T_c$ , and  $T_c$  is the fixed duration of each element of the time-hopping sequence. In order to achieve proper synchronization and to avoid ambiguities with the staggering of the PRI, the following conditions must be satisfied for the signal structure given in (11),

$$|\varepsilon_n T_c| \leq T_r/2, \quad T_c \ll T_r, \quad T_r \geq 2\Delta T. \quad (12)$$

Due to the fact that the energy spectrum of the GGP signal is characterized by the combination of significant low-frequency content as well as ultra-wide frequency bandwidth, the signal model  $s(t)$  given in (11) is very attractive for the applications of ground-probing radar (GPR), foliage-penetration radar (FPR), line-of-sight all-weather radar, high-resolution synthetic aperture radar (SAR), and multiple-access radio communications [15–18]. Performance evaluation of the signal model  $s(t)$ , in terms of range-velocity resolution and clutter-suppression capabilities, can be accomplished by deriving the ambiguity function and analyzing it for different signal parameters and coding structures.

## 2.4. Doppler-Effect of Carrier-Free Signals

In order to derive the ambiguity function for the signal model given in (11), we must first describe the Doppler-effect associated with target motion and carrier-free nonsinusoidal signals. For the narrow-band sinusoidal signal given in (2), the Doppler-effect is recognized by a shift of the transmitted carrier frequency  $f_o$  to a frequency  $\tilde{f}_o = f_o + f_d$  for the received signal from a moving target with a constant velocity. Generally, the Doppler-frequency shift  $f_d$  is given by the relationship

$$\tilde{f}_o = f_o \left(1 - \frac{2v_r}{c}\right), \quad f_d = -2f_o v_r/c, \quad (13)$$

where  $c$  is speed of light, and  $v_r$  is the radial velocity of target relative to radar. For a receding (opening) target, the radial velocity  $v_r > 0$ , and the Doppler-frequency shift  $\tilde{f}_o < f_o$ . On the other hand, an approaching (closing) target with  $v_r < 0$  yields  $\tilde{f}_o > f_o$ . The Doppler effect also causes distortion of the modulation envelope of the radar signal.

For the carrier-free signal  $s(t)$  given in (11), the Doppler effect is expressed by a change (in the form of contraction or spreading) of the effective duration  $\Delta T$  of each component GGP, the PRI  $T_r$ , and the duration  $T_c$  of the time-hopping code element. In addition to the Doppler-time dilation, the amplitude of each pulse is affected too. In analogy to the Doppler-frequency shift given in (13), the Doppler effect for  $s(t)$  is expressed as follows,

$$\Delta \tilde{T} = \left(1 + \frac{2v_r}{c}\right) \Delta T = \Delta T + \Delta T_d, \quad (14)$$

$$\Delta T_d = \left(\frac{2v_r}{c}\right) \Delta T,$$

$$\tilde{T}_r = \left(1 + \frac{2v_r}{c}\right) T_r = T_r + \Delta T_r, \quad (15)$$

$$\Delta T_r = \left(\frac{2v_r}{c}\right) T_r,$$

$$\tilde{T}_c = \left(1 + \frac{2v_r}{c}\right) T_c = T_c + \Delta T_c, \quad (16)$$

$$\Delta T_c = \left(\frac{2v_r}{c}\right) T_c,$$

$$\tilde{E}_o = E_o \left(1 + \frac{2v_r}{c}\right)^{-1/2}. \quad (17)$$

According to (14)–(16), for a receding target with  $v_r > 0$  the Doppler effect causes spreading of the time intervals  $\Delta T$ ,  $T_r$ , and  $T_c$ , while an approaching target with  $v_r < 0$  causes contraction of these time intervals. Detailed derivations of the Doppler-period shifts given in (14)–(16) are presented in Appendix A. The derivation of the Doppler-amplitude shift given by (17) is derived in Appendix B.

A typical target speed of

$$v_r = 300 \text{ m/s} = 1080 \text{ km/hr},$$

results in the relative speed  $v_r/c = 10^{-6}$ . For the desired pulse widths in the range  $0.1 \text{ ns} \leq \Delta T \leq 1 \text{ ns}$ , the Doppler-period shift  $\Delta T_d$  is negligible and of the order  $0.2 \text{ fs} \leq \Delta T_d \leq 2 \text{ fs}$ . Hence, one may ignore the infinitesimal period  $\Delta T_d$  and set the duration  $\Delta \tilde{T} = \Delta T$ . The PRI  $T_r$  must be as long as signal design can permit in order to achieve a non-negligible Doppler shift  $\Delta T_r$  for enhanced velocity resolution. According to (15), a value of  $T_r = \Delta T c/2v_r$  yields a Doppler effect  $\Delta T_r = \Delta T$ . For pulse durations  $0.1 \text{ ns} \leq \Delta T \leq 1 \text{ ns}$  and a relative target speed  $v_r/c = 10^{-6}$ , the PRI must be in the range  $50 \mu\text{s} \leq T_r \leq 0.5 \text{ ms}$ .

### 3. Generalized Ambiguity Function

Based on the Doppler-shifts given in (14)–(17), and the signal model given in (11), the returned signal  $s_r(t)$  from a moving target with a constant relative velocity  $v_r$  can be expressed as follows,

$$s_r(t) = (1 + 2v_r/c)^{-1} \times \sum_{n=0}^{N-1} q_n \Omega_n(t - \tau_r - n\tilde{T}_r - \varepsilon\tilde{T}_c), \quad (18)$$

where  $\tau_r = 2R_o/c$  is the initial range delay described in the derivations given in Appendix A. In practice, the Doppler effects given by (14), (16), and (17) are negligible and they are of no significance to signal resolution. Therefore, we shall assume that  $\Delta\tilde{T} = \Delta T$ ,  $\tilde{T}_c = T_c$ , and  $\tilde{E}_o = E_o$ . These assumptions simplify the form of the received signal given in (18) and yield the relationship,

$$s_r(t) = \sum_{n=0}^{N-1} q_n \Omega_n[t - \tau_r - n(T_r + \Delta T_r) - \varepsilon_n T_c]. \quad (19)$$

The resolution and clutter suppression capabilities of UWB impulse radar can be evaluated by determining the response of a matched-filter receiver to the signal model  $s_r(t)$  given in (19). Since the target parameters  $\tau_r$  and  $\Delta T_r$  are not known a priori at the receiver side, the impulse response of the matched filter must be of the same structure as that given in (19), but with specific range delay  $\tau_f$  and Doppler shift  $\Delta T_f$  instead of  $\tau_r$  and  $\Delta T_r$ . The impulse response  $h(t)$  of the matched filter is expressed as follows,

$$h(t) = \sum_{m=0}^{N-1} q_m \times \Omega_m[T_o - t - \tau_f - m(T_r + \Delta T_f) - \varepsilon_m T_c], \quad (20)$$

where  $T_o$  is a time constant for causality, and

$$\tau_f = 2R_f/c, \quad \Delta T_f = 2T_r v_f/c. \quad (21)$$

In (21),  $R_f$  and  $v_f$  are target range and relative velocity, respectively, to which the receiver filter is matched.

The response function,  $\chi(t)$ , of the matched filter to the received signal  $s_r(t)$  can be determined by the

convolution relationship,

$$\begin{aligned} \chi(t) &= s_r(t) * h(t) = \int_{-\infty}^{+\infty} s_r(\lambda) h(t - \lambda) d\lambda \\ &= \sum_{n=0}^{N-1} \sum_{m=0}^{N-1} q_n q_m \int_{-\infty}^{+\infty} \Omega_n(\lambda - \phi_n^{(r)}) \\ &\quad \times \Omega_m(\lambda - t - \phi_m^{(f)}) d\lambda \\ &= \sum_{n=0}^{N-1} \sum_{m=0}^{N-1} q_n q_m \\ &\quad \times \Upsilon_{nm}[t - (\phi_n^{(r)} - \phi_m^{(f)})], \quad (22) \end{aligned}$$

where the asterisk (\*) denotes convolution and

$$\phi_n^{(r)} = \tau_r + n(T_r + \Delta T_r) + \varepsilon_n T_c, \quad (23)$$

$$\phi_m^{(f)} = \tau_f + m(T_r + \Delta T_f) + \varepsilon_m T_c - T_o. \quad (24)$$

$$\begin{aligned} \Upsilon_{nm}[t - (\phi_n^{(r)} - \phi_m^{(f)})] &= \int_{-\infty}^{+\infty} \Omega_n(\lambda) \\ &\quad \times \Omega_m(\lambda - t + \phi_n^{(r)} - \phi_m^{(f)}) d\lambda. \quad (25) \end{aligned}$$

The function  $\Upsilon_{nm}(t)$  is the cross-correlation function of the two GGP signals  $\Omega_n(t)$  and  $\Omega_m(t)$ . The integral in (25) can be simplified by considering the following substitution:

$$D_r = \Delta T/T_r, \quad D_c = \Delta T/T_c, \quad (26)$$

$$\tau = (t - T_o + \tau_f - \tau_r)/\Delta T, \quad (27)$$

$$\nu = \Delta T_r/\Delta T = 2T_r v_r/c\Delta T, \quad (28)$$

$$\vartheta = \Delta T_f/\Delta T = 2T_f v_f/c\Delta T. \quad (29)$$

In (26), the ratio  $D_r$  is referred to as radar duty cycle, and  $D_c$  time-hopping factor. With the help of the substitutions (26)–(29), the relative time difference  $(t - (\phi_n^{(r)} - \phi_m^{(f)})/\Delta T$  in the integral of (25) can be expressed as follows,

$$\begin{aligned} \varphi(\tau, \nu) &= [t - (\phi_n^{(r)} - \phi_m^{(f)})]/\Delta T \\ &= \tau - (n\nu - m\vartheta) \\ &\quad - (n - m)/D_r - (\varepsilon_n - \varepsilon_m)/D_c. \quad (30) \end{aligned}$$

Insertion of (30) into (22) results in the matched-filter response function

$$\chi(\tau, \nu) = \sum_{n=0}^{N-1} \sum_{m=0}^{N-1} q_n q_m \Upsilon_{nm}(\tau, \nu), \quad (31)$$

$$\Upsilon_{nm}(\tau, \nu) = \int_{-\infty}^{+\infty} \Omega_n(\lambda) \Omega_m(\lambda - \varphi(\tau, \nu)) d\lambda. \quad (32)$$

According to (30), the response function,  $\chi(\tau, \nu)$ , of the matched filter, is a function of target parameters

$\tau$  and  $\nu$ , and radar-design parameters  $D_r, D_c$ , and  $\vartheta$ . The function  $|\chi(\tau, \nu)|$  is referred to as the *generalized ambiguity function* for UWB impulse radar. Although we have based our derivations on the use of the GGP  $\Omega(t)$  as a radar signal, the generalized ambiguity function given in (31) is applicable for any carrier-free signal having the coding structure given in (11).

For coherent pulse modulation we set  $\alpha_n = \alpha$ , and  $\Omega_n(t) = \Omega(t)$  for the signal structure given in (11). In this case,  $\Upsilon_{nm}(t) = \Upsilon(t)$ , where  $\Upsilon(t)$  is the autocorrelation function of  $\Omega(t)$  given in (5). Insertion of (5) into (31) yields the (matched-filter) response function

$$\chi(\tau, \nu) = E_o^2 \Delta T \sum_{n=0}^{N-1} \sum_{m=0}^{N-1} q_n q_m \times \sum_{k=1}^3 I_k \exp\{-a_k [\varphi(\tau, \nu)]^2\}, \quad (33)$$

where  $\varphi(\tau, \nu)$ ,  $I_k$  and  $a_k$  are defined in (30), (6) and (7), respectively.

#### 4. Characteristics of the Generalized Ambiguity Function

According to (33), the generalized ambiguity function is a two-dimensional autocorrelation function in the range-Doppler domain. Analogous to the ambiguity function of conventional radar, the generalized ambiguity function has the following properties:

$$\chi(0, 0) = N\Upsilon(t_o) = N\mathcal{E} = \text{signal energy} \quad (34)$$

$$|\chi(\tau, \nu)| \leq \chi(0, 0), \quad \chi(\tau, 0) = \Upsilon(\tau), \quad (35)$$

$$\int_{-\infty}^{+\infty} \int_{-\infty}^{+\infty} |\chi(\tau, \nu)|^2 d\tau d\nu \leq [\chi(0, 0)]^2 = (N\mathcal{E})^2. \quad (36)$$

Based on the integral relationship given in (36), the volume enclosed by the function  $|\chi(\tau, \nu)|^2$  is constant. Such a property allows for a trade-off between the width of the mainlobe of the function  $|\chi(\tau, \nu)|$  and the height of its sidelobes. In other words, it is possible to have a trade-off between target resolution and clutter suppression.

As we have mentioned earlier, the correlator and the sidelobe canceller in Fig. 2 can be used as a radar receiver for constructing the generalized ambiguity function and enhancing its characteristics. If the impulse response of the correlator in Fig. 2 is set equal to the function  $h(t)$  given in (20), one obtains the response function  $\chi(\tau, \nu)$  at the output terminal of the correlator, the generalized ambiguity function  $|\chi(\tau, \nu)|$

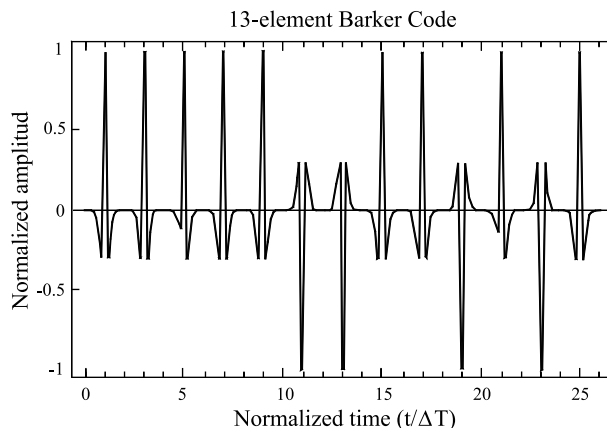


Fig. 4. 13-digit Barker code represented by the signal model given in (10) with code elements  $q_n = \{+1, +1, +1, -1, -1, +1, +1, -1, +1, -1, +1\}$ , scaling factor  $\alpha = 3$ , and duty cycle  $D_r = 0.5$ .

at the output terminal of the full-wave rectifier, and the enhanced ambiguity function

$$\Phi(\tau, \nu) = \chi(\tau, \nu) + |\chi(\tau, \nu)| \quad (37)$$

at the output terminal of the summer. The enhanced ambiguity function  $\Phi(\tau, \nu)$  will be free from the high-level sidelobes associated with the generalized ambiguity function  $|\chi(\tau, \nu)|$ .

To demonstrate the above properties, we consider a 13-element Barker code that is represented by the signal model given in (11), with  $N = 13$ ,  $q_n = \{+1, +1, +1, +1, -1, -1, +1, +1, -1, +1, -1, +1\}$ ,  $\varepsilon_n = \{0\}$ ,  $\alpha = 3$ , and duty cycle  $D_r = 0.05$ . The pulse compression ratio for the coded waveform given in (11) is defined as follows,

$$\eta = \frac{NT_r}{\Delta T} = \frac{N}{D_r}. \quad (38)$$

The 13-element Barker code is shown in Fig. 4, its generalized ambiguity function  $|\chi(\tau, \nu)|$  in Fig. 5(a), and the enhanced ambiguity function  $\Phi(\tau, \nu)$  in Fig. 5(b), for pulse compression ratio  $\eta = 260$ . The plots of Fig. 5 are normalized by the maximum value,  $\chi(0, 0)$ , of the generalized ambiguity function. The normalized correlation functions  $|\chi(\tau, 0)|$  and  $\Phi(\tau, 0)$  are shown in Fig. 6(a) and Fig. 6(b), respectively. The normalized functions  $|\chi(0, \nu)|$  and  $\Phi(0, \nu)$  are shown in Fig. 7. Note that the plot in Fig. 6(a) is the autocorrelation function of the 13-element Barker code shown in Fig. 4. The plot in Fig. 6(b) illustrates the improvement achieved in range resolution, and clutter suppression, by using the sidelobe canceller in Fig. 2. The plots in Fig. 7 show that the levels of sidelobes along the Doppler axis,  $\nu$ , are not affected by the sidelobe canceller.

It is important to mention that by reducing the value of the duty cycle  $D_r$ , which results in a large

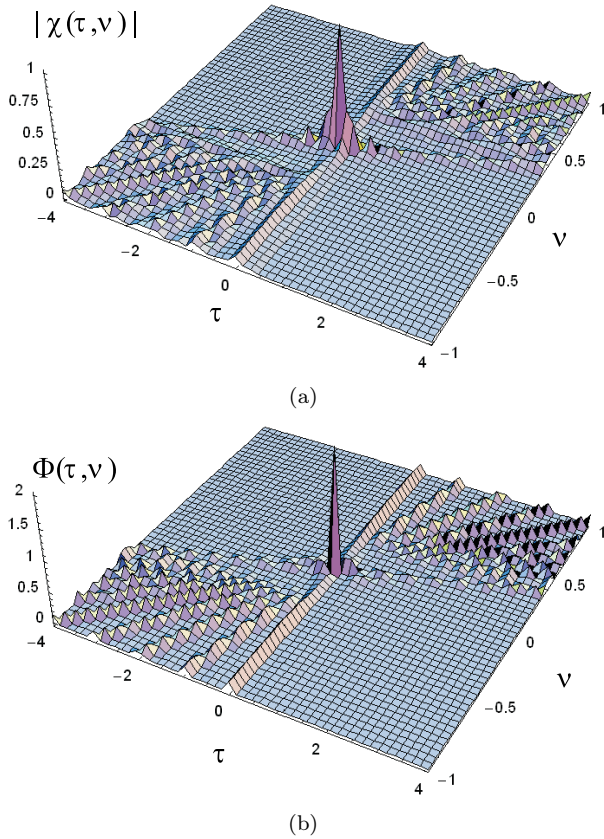


Fig. 5. Generalized ambiguity function  $|\chi(\tau, \nu)|$  (a), and enhanced ambiguity function  $\Phi(\tau, \nu) = |\chi(\tau, \nu)| + \chi(\tau, \nu)$  (b), for 13-element Barker code shown in Fig. 4 having duty cycle  $D_r = 0.05$ .

pulse compression ratio  $\eta$ , causes the sidelobes of the generalized ambiguity function in Fig. 5 to shift away from the vicinity of the mainlobe centered at the origin of the delay-Doppler domain,  $(\tau, \nu)$  [12].

## 5. Conclusions

Nonsinusoidal coded waveforms can analytically be represented as a finite sequence of UWB generalized Gaussian pulses (GGP), whose frequency density spectrum is free from dc component. Theory of radar resolution, in the range and Doppler domain, is developed for nonsinusoidal coded waveforms having the hyperfine structure of GGP signal. Generalized ambiguity function is derived for the performance analysis of UWB impulse radar using coded sequences of GGP signals. The characteristics of the generalized ambiguity function can be enhanced by proper signal design to achieve similar properties of the so called thumbtack ambiguity function, which is a single sidelobe-free impulse in the range-Doppler domain. Such features are desirable for enhanced radar resolution and clutter suppression capabilities.

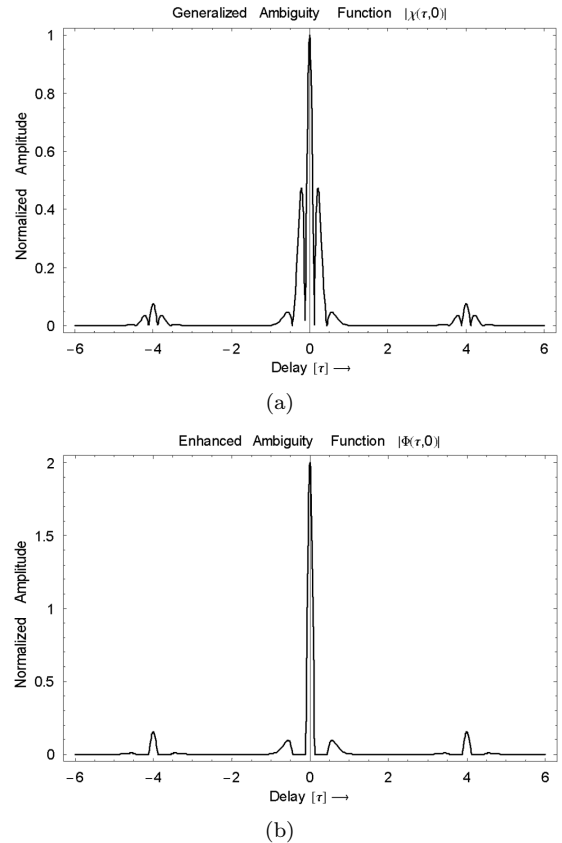


Fig. 6. The correlation function  $|\chi(\tau, 0)|$  (a), and the function  $\Phi(\tau, 0) = |\chi(\tau, 0)| + \chi(\tau, 0)$  (b).

## Appendix A.

The Doppler-shift effect is usually presented in the textbooks of physics in association with the time-harmonic functions. This important phenomenon can also be described by any time function. Consider an ideal (baseband) Gaussian pulse with the time variation

$$g_t(t) = E_o \exp \left\{ -4\pi(t/\Delta T)^2 \right\}, \quad (\text{A.1})$$

where  $E_o$  is the peak amplitude and  $\Delta T$  is the effective duration. Let  $g_t(t)$  be a transmitted radar signal that strikes a point scatterer (or target) at range  $R$  relative to radar. In principle, the reflected signal  $g_r(t)$  received at the radar can be expressed as a delayed version of the transmitted Gaussian pulse  $g_t(t)$ ,

$$\begin{aligned} g_r(t) &= g_t(t - \gamma_t) \\ &= E_o \exp \left\{ -4\pi[(t - \gamma_t)/\Delta T]^2 \right\}, \end{aligned} \quad (\text{A.2})$$

where  $\gamma_t = 2R/c$  is the round-trip propagation delay. For a steady target motion that yields a change in the range  $R = R(t)$  during the period the transmitted signal is being reflected back to radar, the range delay  $\gamma_t$  can be expressed as a Taylor series expansion about

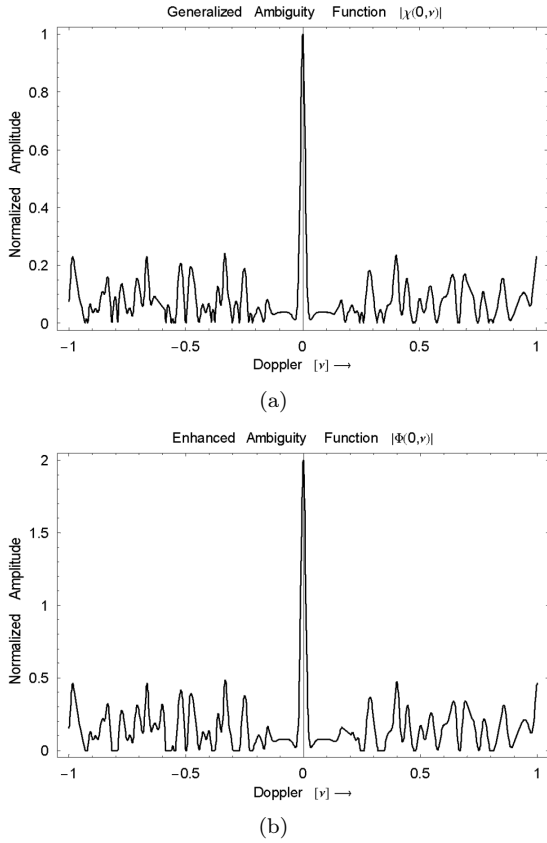


Fig. 7. The function  $|\chi(0, \nu)|$  (a), and the function  $\Phi(0, \nu) = |\chi(0, \nu)| + \chi(0, \nu)$  (b).

a reference time delay  $\tau_o$ ,

$$\begin{aligned} \gamma_t = \tau_o + (t - \tau_o) \frac{2v_r}{c} \\ + \frac{(t - \tau_o)^2}{2!} \frac{2a_r}{c} + \frac{(t - \tau_o)^3}{3!} \frac{2\dot{a}_r}{c} + \dots \end{aligned} \quad (\text{A.3})$$

In (A.3),  $\tau_o = 2R_o/c$  is an initial range delay,  $v_r = \dot{R} = dR(t)/dt$  is radial velocity relative to radar,  $a_r = \ddot{R} = d^2R(t)/dt^2$  is radial acceleration, etc. Based on the series expansion given in (A.3), we write the relative time difference  $(t - \gamma_t)/\Delta T$  in terms of the initial range delay and the range rates as follows,

$$\begin{aligned} \frac{t - \gamma_t}{\Delta T} = \frac{t - \tau_o}{\Delta T} \left[ 1 - \frac{2v_r}{c} - \frac{(t - \tau_o)}{2!} \frac{2a_r}{c} \right. \\ \left. - \frac{(t - \tau_o)^2}{3!} \frac{2\dot{a}_r}{c} - \dots \right]. \end{aligned} \quad (\text{A.4})$$

According to (A.4), target motion causes a Doppler effect that is recognized by a *scaling* of the time axis. The Doppler-scaling factor is a function of the range derivatives. Insertion of (A.4) into (A.2) will show that the effective duration  $\Delta\tilde{T}$  of the returned signal  $g_r(t)$  is equal to a dilated (or contracted) version of the

effective duration  $\Delta T$  of the transmitted signal  $g_t(t)$ ,

$$\begin{aligned} \Delta\tilde{T} = \left[ 1 - \frac{2v_r}{c} - \frac{(t - \tau_o)}{2!} \frac{2a_r}{c} \right. \\ \left. - \frac{(t - \tau_o)^2}{3!} \frac{2\dot{a}_r}{c} - \dots \right]^{-1} \Delta T. \end{aligned} \quad (\text{A.5})$$

For a steady target motion with constant radial velocity  $v_r$  and zero higher-order range derivatives,  $a_r = \dot{a}_r = 0$ , the duration  $\Delta\tilde{T}$  of the returned signal can be expressed as follows,

$$\begin{aligned} \Delta\tilde{T} &= \left( 1 - \frac{2v_r}{c} \right)^{-1} \Delta T \approx \left( 1 + \frac{2v_r}{c} \right) \Delta T \\ &= \Delta T + \Delta T_d, \\ \Delta T_d &= \frac{2v_r}{c} \Delta T, \text{ for } \frac{2v_r}{c} \ll 1. \end{aligned} \quad (\text{A.6})$$

where the duration  $\Delta T_d$  is the Doppler-period shift. For the signal model  $s(t)$  given in (11), the Doppler effect will cause dilation (or contraction) of the PRI  $T_r$  and the duration  $T_c$  corresponding to the time-hopping code. In analogy to (A.4), the Doppler effect transforms the relative time axis

$$(t - \gamma_t - nT_r - \varepsilon_n T_c) / \Delta T$$

into  $t - \tau_o - n\tilde{T}_r - \varepsilon_n \tilde{T}_c) / \Delta\tilde{T}$ , where

$$\begin{aligned} \tilde{T}_r = \left[ 1 - \frac{2v_r}{c} - \frac{(t - \tau_o)}{2!} \frac{2a_r}{c} \right. \\ \left. - \frac{(t - \tau_o)^2}{3!} \frac{2\dot{a}_r}{c} - \dots \right]^{-1} T_r \end{aligned} \quad (\text{A.7})$$

$$\begin{aligned} \tilde{T}_c = \left[ 1 - \frac{2v_r}{c} - \frac{(t - \tau_o)}{2!} \frac{2a_r}{c} \right. \\ \left. - \frac{(t - \tau_o)^2}{3!} \frac{2\dot{a}_r}{c} - \dots \right]^{-1} T_c. \end{aligned} \quad (\text{A.8})$$

For a constant target velocity  $v_r$  and zero target acceleration  $a_r = 0$ , the relationships in (A.7) and (A.8) reduce to the following forms

$$\begin{aligned} \tilde{T}_r &= \left( 1 - \frac{2v_r}{c} \right)^{-1} T_r \approx \left( 1 + \frac{2v_r}{c} \right) T_r \\ &= T_r + \Delta T_r, \\ \Delta T_r &= \frac{2v_r}{c} T_r, \text{ for } \frac{2v_r}{c} \ll 1. \end{aligned} \quad (\text{A.9})$$

$$\begin{aligned} \tilde{T}_c &= \left( 1 - \frac{2v_r}{c} \right)^{-1} T_c \approx \left( 1 + \frac{2v_r}{c} \right) T_c \\ &= T_c + \Delta T_c, \\ \Delta T_c &= \frac{2v_r}{c} T_c, \text{ for } \frac{2v_r}{c} \ll 1. \end{aligned} \quad (\text{A.10})$$

where  $\Delta T_r$  and  $\Delta T_c$  are the Doppler-period shifts corresponding to  $T_r$  and  $T_c$ , respectively.

## Appendix B.

Target motion not only causes a Doppler-period shift, as we demonstrated in Appendix A, but it also yields a Doppler-amplitude shift. In compliance with the *law of the conservation of energy*, the *effective weight* of the transmitted signal and that of the reflected signal from a moving target must be equal, assuming ideal propagation and reflection conditions. We refer to the product of the signal peak amplitude and effective duration as the effective weight. To elucidate this fact, we express the transmitted signal  $g_t(t)$  in terms of the inverse Fourier transform integral,

$$g_t(t) = \int_{-\infty}^{+\infty} G_t(f) \exp\{j2\pi ft\} df, \quad (\text{B.1})$$

where  $G_t(f)$  is the Fourier transform of  $g_t(t)$ . Since in the frequency domain the Doppler effect can be expressed by the frequency transformation

$$\tilde{f} = (1 - 2v_r/c)f,$$

the frequency spectrum  $G_t(f)$  can be transformed into  $G_t(\tilde{f}/(1 - 2v_r/c))$  as a cause of the Doppler effect. In this case, the returned signal  $g_r(t)$  can be expressed in terms of the inverse Fourier transform integral

$$g_r(t) = \int_{-\infty}^{+\infty} G_t\left(\frac{\tilde{f}}{1 - 2v_r/c}\right) \exp\{j2\pi\tilde{f}t\} d\tilde{f}. \quad (\text{B.2})$$

With the change of variables  $\hat{f} = \tilde{f}/(1 - 2v_r/c)$ , one obtains the relationship

$$\begin{aligned} g_r(t) &= \left(1 - \frac{2v_r}{c}\right) \int_{-\infty}^{+\infty} G_t(\hat{f}) \\ &\quad \times \exp\left\{j2\pi\hat{f}\left(1 - \frac{2v_r}{c}\right)t\right\} d\hat{f} \\ &= \left(1 - \frac{2v_r}{c}\right) g_t\left[\left(1 - \frac{2v_r}{c}\right)t\right] \\ &\approx \left(1 + \frac{2v_r}{c}\right)^{-1} g_t\left(\frac{t}{1 + 2v_r/c}\right), \\ &\quad \text{for } \frac{2v_r}{c} \ll 1. \quad (\text{B.3}) \end{aligned}$$

Substitution for  $g_t(t)$  from (A.1) into (B.3) results

in the complete expression for the returned signal  $g_r(t)$ ,

$$\begin{aligned} g_r(t) &= \left(1 + \frac{2v_r}{c}\right)^{-1} E_o \\ &\quad \times \exp\left\{-4\pi\left[\frac{(t - \tau_o)}{(1 + 2v_r/c)\Delta T}\right]^2\right\} \\ &= \tilde{E}_o \exp\left\{-4\pi\left[\frac{(t - \tau_o)}{\Delta\tilde{T}}\right]^2\right\}, \quad (\text{B.4}) \end{aligned}$$

where  $\tilde{E}_o = E_o/[1 + (2v_r/c)]$  and

$$\Delta\tilde{T} = [1 + (2v_r/c)]\Delta T.$$

According to (A.1) and (B.4), the weight  $W = E_o\Delta T$  of the transmitted Gaussian pulse  $g_t(t)$  equal to the weight of the returned signal,  $\tilde{W} = \tilde{E}_o\Delta\tilde{T} = E_o\Delta T$ , which satisfies the law of conservation of energy.

Manuscript received July 07, 2006

## References

- [1] Harmuth H.F. Nonsinusoidal Waves for Radar and Radio Communications. – New York: Academic. – 1981.
- [2] Taylor J.D. (Editor), Introduction to Ultrawideband radar Systems. – Florida: CRC Press: – 1995.
- [3] Smith P.D. and Cloude S.R. (Editors), Ultrawideband, Short-Pulse, Electromagnetics. – New York: Kluwer Academics/Plenum Publishers. – 2002.
- [4] Ville J. Theory and application of the notion of the complex signal // Câbles et Transmission – 1948. – V. 2. – P. 67–74.
- [5] Woodward P.M. Probability and Information Theory with Application to Radar. – New York: McGraw-Hill. – 1953.
- [6] Cook C.E. and Bernfield M. Radar Signals. – New York: Academic. – 1967.
- [7] Rihaczek A.W. Principles of High Resolution Radar. – New York: McGraw-Hill. – 1969.
- [8] Costas J.P. A study of a class of detection waveforms having nearly ideal range-doppler ambiguity function // Proc. IEEE – Aug. 1984. – V. 27, № 8. – P. 996–1009,
- [9] Rihaczek A.W. Delay-Doppler ambiguity function for wideband signals // IEEE Trans. AES – July 1967. – V. AES-3, № 4. – P. 705–711.

- [10] Deley G.W. Waveform Design. In Radar Handbook M.I. Skolnik, ed. – New York: McGraw-Hill. – 1970.
- [11] Harmuth H. F. Synthetic apertur radar based on nonsinusoidal functions. VII: Thumbtack ambiguity function // IEEE Trans.Electromagn. Compat. – Aug. 1980. – V. EMC-22, №. 3. – P. 181–190,
- [12] Hussain M. G. M. Principles of high-resolution radar based on Nonsinusoidal waves-Part II: Generalized ambiguity function // IEEE Trans.Electromagn. Compat. – Nov. 1989. – V. EMC-31, №. 4. – P. 369–375.
- [13] Hussain M. G. M. Principles of space-time array processing for ultra-wideband impulse radar and wireless communications // IEEE Trans.Veh. Technol. – May 2002. – V. 51, №. 3. – P. 393–403.
- [14] Hussain M. G. M. Antenna patterns for nonsinusoidal waves with the time variation of a Gaussian pulse-Part I// IEEE Trans. Electromagn. Combat. – Nov. 1988. – V. EMC-30, №. 4. – P. 504–512.
- [15] Astanin L.Y. and Kostylev A.A. Ultrawideband Radar Measurements: Analysis and Processing. – London: IEE Press. – 1999.
- [16] Win M.Z. and Scholtz R.A. Impulse radio: How it works // IEEE comms. Letters – Feb. 1998. – V. 2, №. 2. – P. 36–38.
- [17] Hussain M.G.M. Ultra-wideband impulse radar- An overview of pinciples // IEEE AES Magazine – Sept. 1998. – V. 13, №. 9. – P. 9–14.
- [18] Hussain M.G.M. Principles of high-resolution radar based on Nonsinusoidal waves-Part I: Signal representation and pulse compression // IEEE Trans.Electromagn. Compat. – Nov. 1989. – V. EMC-31, №. 4. – P. 359–368.